The use of red blood cells to map wall shear and flow separation

Justin D. Bingham, William Wangard III, David S. Dandy[†]

Department of Chemical Engineering, Colorado State University, Fort Collins, CO 80523-1370, USA

Abstract

Laminar flow boundary layer separation in channel flow has been experimentally and numerically investigated. An experimental method was developed incorporating the use of wall-attached and dispersed canine red blood cells to quantify the local wall shear stress, and to determine the presence and location of flow separation and attachment. A master curve relating wall shear stress to attached cell elongation was generated. Measurement of the cell elongation was accomplished via image analysis software, which lent to the accuracy and sensitivity of the method. Parallel plate flow experiments were performed using obstacle geometries that lead to both two- and three-dimensional flow separation. Using this experimental technique the existence of flow separation, location of flow separation and attachment, and magnitude and direction of the local wall shear stress were all accurately quantified as functions of the Reynolds number. Computational fluid dynamics simulations of the flow experiments were performed, the results of which exhibited close quantitative agreement with the experiments. Numerical and experimental results were used to examine unresolved issues in three-dimensional flow separation. The results support the hypothesis that, for three-dimensional separation, there is no explicit mathematical link between the location of the surface separation line and the magnitude of the local wall shear stress. It was observed that singular separation and attachment points were accompanied by vanishing normal components of the wall pressure gradient. It was verified by the experiments that ordinary flow separation lines originate from singular separation points.

[†] david.dandy@colostate.edu

Keywords: Laminar flow; fluid mechanics; suspension; momentum transfer; boundary layer separation; wall shear.

1. Introduction

The phenomenon of separated flow represents a domain of fluid mechanics of great practical interest. Separation can be a controlling and often dominant feature of many fluid flows. For flow over bluff bodies, for example, the location of separation significantly influences the form drag on the body. Similarly, flowing particle concentration techniques such as inertial migration based branched tube separators, and even reacting flow processes such as catalytic combustion and chemical vapor deposition, are sensitive to the effects of flow separation. In many cases, separation can drastically alter the flow field and hence the performance of a particular device. Consequently, understanding the nature of these flows and providing an effective and accurate means of experimentally locating where separation occurs would be of significant interest in various applications. In addition to the usefulness of such knowledge in practical applications, a sound understanding of three-dimensional flow separation is desired from a purely fundamental fluid mechanics perspective.

Flow separation is of fundamental importance in many fluid flows. For flow over bodies or in confined channels, when the imposed pressure gradient is adverse the thickness of the viscous boundary layer increases as momentum is consumed by both pressure gradient and wall shear, and at some point, the viscous layer may break away, or separate from the bounding surface (Williams, 1977). The point or line where the boundary layer breaks away from the surface and separates the region of downstream-directed flow from the region of recirculating flow is known as the separation point or separation line.

For two-dimensional flow separation, the point of separation coincides with the point of vanishing tangential wall shear stress. Consequently, the point of vanishing shear has been taken for years as an indicator of separation or attachment. For three-dimensional flow, however, separation does not necessarily coincide with a point or line of vanishing wall shear, hence a general definition of separation that includes only vanishing wall shear is not sufficient. Due to the additional velocity component and extra spatial dimension in three-dimensional flow, separation can occur through one or both of two routes. The first mechanism, termed singular separation, occurs when both principal components of the wall

shear stress vanish at the same point. The second route, referred to as ordinary or regular separation, occurs when the streamline projections converge asymptotically on either side of a surface separation line. At present there exist unresolved issues associated with separation in three-dimensional flows. First, there is no *a priori* connection between the location of separation and the values of the surface shear stress components. Also, the extent to which the pressure distribution alters the location of separation, or vice versa, is not fully understood.

To explore these issues, an experimental technique is used which incorporates surface-attached canine red blood cells as a mechanical tracer to quantitatively measure wall shear stress in regions of flow separation. Because of some initial work directed at understanding and characterizing the mechanical properties of the erythrocyte membrane, it is recognized that the red blood cell is particularly well suited to the mapping of wall shear stress (Hochmuth, Mohandas & Blackshear, 1973; Rakow & Hochmuth, 1975a; Rakow & Hochmuth, 1975b). In those studies, carried out in parallel plate flow geometries, red cells were attached to the wall of a chamber and isotonic saline was passed through the chamber under laminar conditions. The resulting unidirectional flow provided a well-characterized shear stress at the walls while at the same time uniformly deforming the attached cells. By mounting the flow chamber on the stage of a microscope, the deformation, or elongation of the attached cells could be observed and measured. Once the flow was stopped the cells recovered their original circular, biconcave shape. Most of the early red blood cell studies involved human cells, but Hung, Shen, Akutsu & Hwang (1978) extended the attached-cell approach to obtain stress-elongation curves for both point-attached and line-attached canine erythrocytes. Examples of these two types of cell attachment are shown schematically in Fig. 1.

A number of established alternative techniques exist for measuring shear stress at or near walls (Ackerman, Wong, Ethier, Allen & Spelt, 1994; Hayashi, Yanai & Nakai, 1996; Yamaguchi & Hanai, 1987; Haguwara, Esmaeilzadeh, Tsutsui & Suzuki, 1989; Gür & Leehey, 1989). However, they all share a number of drawbacks, and none can readily be used in systems where geometrical constraints are present. Unlike most existing methods for measuring wall shear, the red blood cell tracer technique is essentially noninvasive because of the relatively small cell thickness, and the extent of surface-attached cell

deformation can be converted directly to wall shear stress. Also, this technique not only gives magnitude of the shear stress, but direction can be easily discerned as well. In addition, the red blood cell tracer allows for a near-continuous surface shear map, which, when combined with the other advantages, makes a strong argument for the use of this technique, especially for mapping zero shear boundaries in a flow system.

In this study experiments have been carried out using the attachment of canine red blood cells to the glass surface of a parallel plate flow chamber as a diagnostic for shear stress magnitude as well as flow direction, with a particular focus on the study of shear stress and flow separation. To use cell elongation as a quantitative measure of wall shear stress it is necessary to first generate a master curve of wall shear stress versus cell elongation. This has been accomplished by exposing the attached cells to a well-characterized flow and measuring their deformation by optical microscopy and image processing software. Further experiments were performed utilizing channel geometries conducive to two- and three-dimensional flow separation. Although 2D separation is viewed as a well-understood phenomenon, it was used in the present study as a means of validating the experimental technique and of benchmarking the fluid dynamics simulations discussed below. Two-dimensional separation was achieved by placing an obstacle cross-wise to the flow in the channel, while for 3D flow a vertical obstruction was used and this generated a laminar horseshoe vortex. This 3D configuration was chosen because the horseshoe vortex formed around the base of a vertical cylinder by a separating laminar boundary layer has been previously studied in detail (Coon & Tobak, 1995; Baker, 1991; Baker, 1979). Since the boundary layer is known to undergo three-dimensional separation at some distance upstream from the cylinder/plate junction, this type of flow was used as an experimental means of reproducing three-dimensional flow separation in the present study.

At the same time, computational fluid dynamics calculations were carried out to predict the structure and location of separated flows in the corresponding experiments, and to link the wall shear stress measurements to the locations of surface separation/attachment lines and vanishing shear stress points. The numerical analysis was also used to further verify the quantitative nature of the experimental

technique and to address unresolved issues associated with three-dimensional flow separation, including the role of pressure and derivatives of pressure. A great deal of numerical and experimental work related to 3D flow separation has been done (e.g., Dandy & Dwyer, 1990; Cherukat, McLaughlin & Dandy, 1999; Rogers, Kaul & Kwak, 1997; Kaul, Kwak & Wagner, 1985; Kiehm, Mitra & Fiebig, 1986; Kwak, Rogers, Kaul & Chang, 1986; Lee, Chiu & Jen, 1997; Lee & Chiu, 1992). However, very few papers exist that utilize both numerical simulation and experimental observation in the same study. With this combined approach the present work seeks to elucidate some important unresolved issues associated with three-dimensional flow separation.

2. Methodology

The experimental portion of this study can be divided into three categories. The first set of experiments involves the generation of a master stress versus elongation curve relating the deformation or elongation of the attached red blood cells to the shear stress at the wall. The second set involves the study of the flow in a geometry where two-dimensional flow separation occurs. And finally, the third class of experiments concerns analysis of the flow field in a geometry that exhibits three-dimensional flow separation. The principal difference between the three sets of experiments was the interior geometry of the flow channel. All experiments involved the attachment of canine red blood cells to the bottom plate of the flow channel and the subsequent analysis of the extent of deformation of attached red blood cells subjected to different Reynolds number flows.

2.1. Flow channel assembly and general techniques

A parallel plate flow chamber was used in all the experiments. The flow chamber was designed to fit on the stage of a microscope, allowing real time analysis of the red blood cell deformation as the experiments were conducted. As illustrated in Fig. 2, the flow area itself consisted of a plastic laboratory film gasket sandwiched between two glass microscope slides. In such a manner, the plastic gasket served as the vertical walls of the flow channel and the channel height could be varied via stacking multiple

gaskets. Two holes were drilled in the bottom glass slide to provide an inlet and outlet for the flowing fluid. The gasket and glass slides were secured between a bottom plastic plate and a top steel plate.

The canine red blood cells were collected from the dogs on the same day that experiments were to be performed. The blood samples were collected and treated with ethylene diamine tetra-acetic acid (EDTA) to prevent coagulation. The whole blood was then centrifuged for 5 minutes to separate the red blood cells from the plasma. After removing the plasma from the settled red blood cells, the cells were washed in phosphate-buffered saline (PBS with *p*H 7.4 and approximately 260 mOsm). Again the samples were spun down for 5 minutes, after which the PBS was aspirated off the settled cells. The cells were washed with PBS one to two more times. Finally the washed cells were re-suspended at a hematocrit of approximately 0.5% in PBS containing 0.1% dextrose.

In all of the experiments, before introduction of the cell suspension into the flow chamber, the chamber was flushed with PBS. The cell suspension was then introduced into the flow chamber via a manual syringe connected to a bivalve that in turn was connected to the bottom plastic plate of the assembled channel (cf. Fig. 2). The cells were allowed to settle and attach on the bottom glass surface of the flow chamber for 5 to 10 minutes. The attached cells were then subjected to a constant fluid shear stress, τ, by introduction of a cell-free PBS solution from the upstream end of the flow channel. A variable speed syringe pump was used to control the flow rate of the incoming PBS solution. The unused valve on the bivalve served as the inlet connection for the syringe-pump-controlled PBS flow.

The assembled channel, along with all the inlet and outlet connections, was placed on the stage of an optical microscope. Cells attached to the bottom glass surface of the channel, as well as the patterns of unattached free flowing cells, were continuously observed in transmission mode at magnifications of 50X, 100X, 200X, and 400X. Still photographs and video recordings were utilized to record information from the experiments.

2.2. Master stress-elongation curve experiments

To use the attached cells in a study of separation it is necessary to first generate data on the extent of cell deformation as a function of the known shear stress the attached red blood cells experienced at the wall in a well characterized flow field, that is, to obtain a stress-elongation curve for the cells. This data would then be used in subsequent experiments involving more complicated interior geometries where the shear stress at the wall was not known. For simplicity and reproducibility, the data for the stress-elongation curve were collected only for the red blood cells that exhibited point-attachment on the bottom glass plate of the flow chamber.

In this study the interior of the flow chamber had a height h = 0.023 cm, width w = 0.825 cm, and length ℓ = 4.2 cm. For the Reynolds numbers considered here it is estimated that the entrance length ℓ_e was short, so that the flow was fully developed within approximately 0.1 cm of the inlet. Thus, because $\ell_e \ll \ell$ and $h/w \ll 1$, near the midpoint of the device where the measurements were taken the flow was nearly unidirectional (White, 1986) and the tangential stress, τ, acting on the free surface of the attached cells was taken from the parallel-plate Poiseuille flow result (Hung et al., 1978), $\tau = 6\mu(h-2T)Q/wh^3$. In this expression μ is the viscosity of the fluid, Q is the volumetric flow rate, and T is the cell thickness. The viscosity of the PBS solution was assumed to be equal to that of water at 101.3 kPa and 298 K, 8.9×10^{-4} N·s·m^{-2} (Hardy & Cottington, 1949). Since the cell thickness was much less than the height of the channel ($T \approx 2$ μm), the expression relating wall shear stress to flow rate can be simplified to $\tau = 6\mu Q/wh^2$. For a specified flow rate the stress predicted by this equation is associated with measured cell deformation, and in this manner a master curve can be generated.

After washing and preparing the flow chamber for the experiments, the cell suspension was injected and allowed 5 to 10 minutes to settle on the bottom glass slide. Pictures were taken of the attached cells with no flow at magnification 400X, that is, in their undeformed state L_o. A known flow rate was then imposed and photographs of the cells were taken in their elongated state, L, which was the length of the major axis for the point-attached cells. The flow rate Q was varied via the syringe pump from 0 to

0.2 mℓ/sec, resulting in a wall shear stress range of 0 to 20 dyn/cm^2. All experiments were performed at room temperature (298 ±2 K). The photographs of the cells were scanned at 600 dpi resolution and analyzed with image processing software. In this manner the undeformed cell diameter, L_o, as well as the elongated cell length, L, could be measured accurately. A relationship was thus found relating the wall shear stress, τ_w, to the measured dimensionless cell elongation, $\lambda = L/L_o$.

2.3. Two-dimensional flow separation experiments

Experiments were performed in the flow device shown in Fig. 2, with the addition of a horizontal cylindrical obstacle, oriented across the width of the channel and attached to the bottom plate. A 25-gauge wire (diameter d = 0.041 cm) was glued to the glass, and after drying excess glue was mechanically removed. The plastic gasket was then placed over the wire and sandwiched between the two slides while heating the overhanging ends of the wire. In this way, the plastic melted and formed around the heated wire. After the plastic was melted around the wire, a layer of adhesive was applied to the plastic/wire interface to form a barrier for fluid entry, and the device was then assembled. Its interior dimensions were h = 0.061 cm, w = 0.95 cm, and ℓ = 4.2 cm. Flow through this configuration was observed to be nearly two dimensional for the range of Reynolds numbers studied, particularly in the central region away from both the sidewalls and the inlet and outlet.

During each experiment the cell suspension was introduced into the clean channel and allowed to settle. Photographs of the undeformed attached cells were taken, as well as images of the attached cells deforming due the flow of PBS. The photographs were taken in the regions of flow separation and attachment, which were evident by the magnitude and direction of deformation of the attached cells. These regions were also visualized on video since some of the unattached free-flowing cells would get caught in, and subsequently trace out, the recirculation regions. Data were collected at three different flow rates, that is, different Reynolds numbers corresponding to Re = 8.7, 23.9, and 44.6. To define the Reynolds number, the diameter of the cylinder, d, was used as the characteristic length, rather than the

channel height h, such that $Re = \langle u \rangle d/\nu$, where $\langle u \rangle$ is the average velocity based on flow rate, and as mentioned above, ν is taken to be the kinematic viscosity of water at room temperature.

For all three Reynolds numbers, data were gathered for the determination of separation and attachment locations relative to the obstacle, as well as magnitude of wall shear stress in the regions of such flows. Since the diameter of the cylinder was known, it was used as a reference length in the video and photographs to quantify the distance upstream and downstream that flow separation and attachment occurred. In these regions, photographs of the cells were taken at 400X and later scanned into image processing software to measure λ, the deformed cell length relative to the undeformed cell diameter, and this in turn was used to determine the corresponding wall shear stress using the master stress-elongation curve.

2.4. Three-dimensional flow separation experiments

To obtain a three-dimensional horseshoe vortex flow a vertical cylinder was mounted on the bottom plate of the flow device. The cylinder was cut from galvanized steel wire (diameter $D = 0.08$ cm) and both end surfaces were smoothed and squared. The finished cylinder was then attached to the bottom glass slide with adhesive, and after drying the excess glue was removed. The height of the cylindrical obstacle was 0.09 cm and the physical dimensions of the channel used for the experiments were $h = 0.14$ cm, $w = 1.0$ cm, and $\ell = 4.2$ cm. A detailed study of the wall shear magnitude in the region of flow separation was performed for three different Reynolds number flows corresponding to $Re = 22.5$, 31.5, and 44.1, where the Reynolds number was based on the cylinder diameter D. As with the two-dimensional flow experiments, photographs and video recording of the experiments were used to capture the necessary data.

2.5. Two-dimensional flow simulations

In the two-dimensional flow simulations, the numerical method utilized a conservative finite difference technique implemented on overlapping grids using Overture (Henshaw, 1998), an object

oriented software framework for solving coupled sets of differential equations on overlapping grids. Included in this software framework is an overlapping grid generator, Ogen, and a post-processor, PlotStuff, used to visualize data on overlapping grids generated by Overture. The overlapping grid used was comprised of a background Cartesian grid and a hyperbolic, boundary-fitted grid generated from a spline surface to match the contours of the bottom plate and cylinder. The two-dimensional continuity and Navier-Stokes equations were solved in primitive variables form. The inlet velocity was specified as parabolic inflow. Homogeneous Dirichlet boundary conditions were used for all velocity components on no slip walls. The outlet condition was homogeneous Neumann on all velocity components. For the pressure, homogeneous Dirichlet boundary conditions at the outflow, and homogeneous Neumann conditions at the inflow and no slip walls were used. The pressure was specified at the outlet as an initial pressure condition and remained constant throughout the simulations.

The solver used, LINS3D (Wangard, 1999), was based on a projection method using a Poisson equation to correct the pressure and in turn the velocity. The solver was fully implicit whereby the convective operator in the Navier-Stokes equations was linearized using the velocity from the previous time step. The steady velocity and pressure fields were thus computed and, via numerical differencing, the shear stress at the wall τ_w was calculated. The convergence criteria for the algorithm were that the maximum relative change the velocity components between iterations must be smaller than 10^{-4}, the maximum relative change in the pressure correction factor must be less than 10^{-3}, and the continuity equation must be satisfied to within one part in 10^4.

2.6. Three-dimensional flow simulations

The three-dimensional flow separation experiments were simulated using the commercial package FLUENT 5. The grid was generated using an application called Gambit, and then read into FLUENT where further grid adaptation was performed. The grid consisted of an unstructured mesh with a refined boundary layer region constructed around the cylinder to accurately capture the flow separation phenomena. For each Reynolds number, an appropriate parabolic velocity profile was defined for the inlet

condition. The no slip boundary condition was specified on all walls. The convergence criterion was that the relative change in the continuity equation between iterations must be smaller than 10^{-4}.

3. Results

3.1. Master stress-elongation curve

Data on the extent of surface-attached red blood cell deformation were collected as a function of wall shear stress, and the result is shown in Fig. 3. In this figure, L represents the major axis length of the deformed cell, and L_o is the undeformed diameter. Each point in Fig. 3 represents the average elongation $\lambda = L/L_o$ values of 15 to 20 different point-attached red blood cells exposed a known wall shear stress, τ_w. The error bars associated with each point represents two standard deviations of the data collected for that sample. To avoid the necessity of using extrapolation when applying this data to unknown flow fields a fourth order polynomial was fit to the averaged data. It is believed that the error bars, representing ± 1 standard deviation, associated with the data in Fig. 3 are a result of the samples having a distribution of undeformed cell diameters. Because a larger cell has more surface area exposed to external forces, specifically, fluid-induced shear stress, it will deform to a different extent than a smaller cell exposed to the same stress. Thus two cells having different cell diameters L_o would have different elongation values λ when exposed to the same shear stress; this effect would broaden the range of cell elongation values for a given sample and contribute to a large standard deviation.

3.2. Two-dimensional flow separation

Two recirculation zones were typically observed in the two-dimensional flow configuration: a region upstream of the cylinder where the flow separated from the lower wall and reattached to the cylinder surface, and a second region where the flow detached from the downstream half of the cylinder surface and attached to the lower wall further downstream. To quantify how far upstream from the cylinder the flow separated from the wall, and the distance downstream of the cylinder where the flow attached, the experiments were photographed and video taped, and the recirculation regions were visualized by the free

flowing red blood cells that mapped out such regions. To illustrate the nature of the recirculation zones observed in the experiments, streamlines resulting from a computational fluid dynamics simulation at $Re = 23.9$ are shown in Fig. 4, together with the variables used to describe the dimensions of the recirculation regions. Experiments and simulations were also performed for Reynolds numbers of 8.7 and 44.6 to determine how the flow separation and attachment locations varied with Reynolds number. In the figures s represents the distance upstream (negative x-direction) from the centerline of the obstacle to the point where the flow separates from the bottom surface, and a represents the distance downstream (positive x-direction) from the center of the obstacle to the point where the flow attaches to the bottom surface.

All experimental and numerical data for attachment and separation location were normalized using a characteristic length, D, which was chosen to be the distance the cylinder protruded from the wall. Because of the attachment technique it was found that $D > d$. The data for two-dimensional separation and attachment location are presented in Fig. 5. The experimental data agree with the numerical data to within 5.9%. At each Reynolds number, data were collected on the separation and attachment locations for two separate experiments. This is evident from the attachment data, but needs clarification for the separation data since each experimental data point represents two experimentally measured values. Using image analysis software, high magnification photographs (400X) were examined and the extent of attached cell elongation was quantified. Once the cell elongation λ was determined in the regions of flow separation and flow attachment, the master stress-elongation curve was applied to determine the corresponding wall shear stress τ_w. The wall shear stress results for $Re = 23.9$ are given in Fig. 6, together with predicted shear stress values obtained by numerical differencing of the calculated velocity field. Similar data were obtained for $Re = 8.7$ and 44.6. The experimental and theoretical results are in good qualitative agreement, and they differ in magnitude by less than 13% for all three of the Reynolds numbers considered.

3.3. Three-dimensional flow separation

The size of the horseshoe vortex region on the upstream side of the cylinder was quantified as a function of Reynolds number. A photograph illustrating the size and character of the vortex region observed in the experiments is displayed in Fig. 7, in this case corresponding to a Reynolds number of 31.5. Numerical results of path lines traced out by mass-less particles released from the surface line of symmetry are also included in this figure for comparison with the photograph. From the photograph and computational fluid dynamics calculation it is clear that there is a region of fluid around the cylinder—roughly horseshoe shaped—that is isolated from fluid being swept towards the cylinder from upstream. The particle paths in Fig. 7b trace out the *separation line*, that is, the projection onto the lower wall of the limiting stream surface separating the upstream and downstream regions of flow. From the particle pathlines it is not possible to determine the details of how separation occurs from the lower wall. However, by examining the geometry of the attached cells singular separation points can be identified and the behavior of stress along the separation line can be quantified. As shown in the magnified region in Fig. 8 it is evident that there is a very small region on the line of symmetry at the upstream edge of the horseshoe vortex where the cell deformation is zero, and thus the magnitudes of the principal components of wall shear stress vanish. Therefore, this is a point of singular separation and it coincides exactly with the beginning of the horseshoe separation region upstream of the vertical cylinder. Using this approach it was possible to quantify the singular separation location as a function of *Re* by direct measurement of the vortex region thickness. The results for the experimental separation location are shown in Fig. 9, together with the results extracted from the computational fluid dynamics simulations. The experimental data for separation location differ by no more than 0.7% from the numerical predictions. A characteristic length, chosen to be the cylinder diameter D, was used to normalize all experimental and numerical data for flow separation location in the three-dimensional flows. The measured and predicted wall shear stresses along the line of symmetry for the $Re = 31.5$ case are shown in Fig. 10. The upstream separation location may be identified in this figure as the point where τ_w passes through zero, that is, at $x/D \approx -0.94$.

Although both principal components of stress vanish at the locations indicated in Fig. 9, these are the only isolated points on the lower wall where such behavior was observed. It is apparent from experimental visualization and theoretical predictions in this work that separation lines originate from the singular point located on the line of symmetry, but the magnitude of each stress component, τ_{yx} or τ_{yz}, along these regular separation lines is not known *a priori*, nor is the magnitude of the total shear stress, $||\boldsymbol{\tau}_w||$. It was observed qualitatively in all of the experiments that cell elongation increased monotonically along the separation line, reaching a maximum approximately half way around the cylinder, that is, roughly 90° from the upstream line of symmetry. An example of this trend is shown in Fig. 11, where the measured magnitude of total wall shear stress at $Re = 44.1$ is plotted as a function of distance along the separation line (measured in degrees). From Fig. 11 it is evident that the wall shear stress on the surface separation line increases along the front of the horseshoe and then decreases around the downstream side of the vortex region.

The link between pressure, pressure gradient, stress, and flow separation has also been examined. The predicted surface pressure at $Re = 44.1$ along the line of symmetry is displayed in Fig. 12. It was determined that flow separation occurred on this line at a distance $x = –0.08$ cm, or $x/D = –0.99$, upstream of the cylinder center. The point of singular separation clearly does not coincide with any pressure extrema, nor with any extrema in the pressure gradient $\partial P/\partial x$; the maximum in pressure gradient occurs inside the separated region, approximately 0.025 cm upstream of the cylinder surface. However, as Fig. 13 illustrates, the normal component of the pressure gradient, $\partial P/\partial y$, appears to pass through zero at, or at least very near, the point of singular separation. It is not clear at this time whether the discontinuity in the slope of $\partial P/\partial y$ at the separation point is real or an artifact of the first-order, one-sided numerical differencing method. As the point of separation is approached from the upstream side the normal pressure gradient and its derivative are both well behaved.

4. Discussion

4.1. Criteria for 2D and 3D singular flow separation

It is generally accepted that, for two-dimensional flow separation, the point where the flow detaches from the surface is coincident with vanishing wall shear stress. This has been explained mathematically as well as verified experimentally. Somewhat less understood is (are) the condition(s) necessary for three-dimensional flow separation. For three-dimensional singular flow separation it is known that both tangential components of the wall shear stress must vanish simultaneously, because in fact, this is the definition of singular separation. In the regions of three-dimensional separated flow studied in this work, there existed one point on the lower surface that satisfied this condition. This singular point of separation was found to lie on the line of symmetry, thus making the analysis in this plane of symmetry mathematically identical to that for a two-dimensional flow. In addition, the computational fluid dynamics results provided a means of examining the connections between P, $\partial P/\partial x$, $\partial P/\partial y$, and flow separation location along the symmetry line.

Because of the ambiguity of the present results concerning these relationships it is desirable to study the issue of singular flow separation in more detail. In a recent theoretical investigation (Tobak, 1997) it was argued that the point of singular flow separation on a line of symmetry would be preceded by a point where $\omega(x,0) = \omega_x(x,0) = 0$, where ω is the lone non-zero component of vorticity at the surface and the subscript x denotes partial differentiation in the coordinate direction coincident with the symmetry line. Downstream of this "separation onset" point there will a second location where the vorticity vanishes and, according to Tobak, it is at this second point where singular separation or attachment occurs. There is little question that separation or attachment will occur at a point on a surface where both principal shear stress components vanish, but Tobak's hypothesis is very intriguing because it provides a theoretical basis for predicting the onset of such an event. The goal here is to see if the experimental and theoretical results from the present work are consistent with the separation onset criteria. To further examine and discuss this proposed separation condition, a transformation of the equations of motion along the line of

symmetry is carried out to relate the pressure gradient to vorticity. The *x*- and *y*-components of the Navier-Stokes equations may be written in Cartesian coordinates as

$$x: \qquad \rho\left(u_t + u\,u_x + v\,u_y + w\,u_z\right) = -P_x + \mu\left(u_{xx} + u_{yy} + u_{zz}\right) = -P_x + \mu\nabla^2 u \tag{1}$$

$$y: \qquad \rho\left(v_t + u\,v_x + v\,v_y + w\,v_z\right) = -P_y + \mu\left(v_{xx} + v_{yy} + v_{zz}\right) = -P_y + \mu\nabla^2 v\,. \tag{2}$$

On the line of symmetry (x,0,0) the terms on the left-hand sides of Eqs. (1) and (2) vanish since u, v, and w are identically zero at the surface. The right hand side of these equations can be rewritten in terms of the vorticity vector $\boldsymbol{\omega}$ using its definition, which in Cartesian coordinates is

$$\boldsymbol{\omega} = (w_y - v_z)\mathbf{e}_x - (w_x - u_z)\mathbf{e}_y + (v_x - u_y)\mathbf{e}_z\,. \tag{3}$$

On the symmetry line the first four quantities in this expression vanish, resulting in the surface vorticity vector having a single component in the $\mathbf{e}_z$ direction,

$$\omega = v_x - u_y\,. \tag{4}$$

Taking the partial derivative of this expression with respect to x and noting that, on the line of symmetry,

$$\omega_x = v_{xx} - u_{yx} = v_{xx} - (u_x)_y = v_{xx} + v_{yy}\,, \tag{5}$$

since $u_x = -v_y$ due to continuity. Thus it is shown that

$$\omega_x = \nabla^2 v \tag{6}$$

along the line of symmetry. Similarly, starting with Eq. (4) it can be easily shown that $\omega_y = -\nabla^2 u$.

Therefore, on the line of symmetry Eqs. (1) and (2) may be rewritten as

$$P_x = -\mu\,\omega_y \tag{7}$$

$$P_y = \mu\,\omega_x\,. \tag{8}$$

Because the above analysis has been carried out along the line of symmetry, the same result would be obtained on a stationary no-slip boundary in a two-dimensional flow system.

It is apparent from Eq. (8) that, since the x derivative of the vorticity is directly proportional to the y derivative of the pressure, P_y must vanish identically when $\omega_x = 0$. Further, on the line of symmetry the surface vorticity is directly proportional to the surface shear stress. Thus, plots of τ_w ($\equiv \tau_{yx}$) and P_y, from

two-dimensional and three-dimensional (along the symmetry line) simulations, are utilized to address the conditions of separation proposed by Tobak (1997). In other words, by examining the values of P_y and τ_w taken from the data in this work the separation onset condition $\tau_w(x,0) = P_y(x,0) = 0$ proposed by Tobak can investigated for both the two- and three-dimensional flow geometries.

Figure 14 illustrates the behavior of wall shear stress, τ_w, and the normal pressure gradient, P_y, for the two-dimensional flow separation geometry at $Re = 44.6$. For this Reynolds number the point of singular separation occurs at $x/D = -0.65$. While the separation point does coincide with $\tau_w = \omega = 0$, there does not appear to be a point in the immediate vicinity upstream from the singular point where P_y vanishes, which would correspond to a point where $\omega_x = 0$. However, as is evident from the figure, the P_y values have small magnitude in this region and it is possible that the resolution of the numerical method is not sufficient to capture this phenomenon. In any event, these data are inconsistent with the hypothesis proposed by Tobak that both ω_x and τ_w vanish immediately upstream of the separation point.

Figure 15 displays the same quantities for flow along the line of symmetry in the three-dimensional geometry. In this case, flow separation occurred at $x/D = -0.99$. This demonstrates that P_y , and hence ω_x, does vanish in the immediate vicinity of singular flow separation. This behavior of the P_y curve favors the hypothesis proposed by Tobak that singular flow separation is accompanied (or preceded) by a point where the x-derivative of vorticity, ω_x, goes to zero. From the data collected, it is not possible to identify which of the two curves τ_w or P_y cross through zero further upstream. Nevertheless, the stress, and hence the vorticity, is monotonic in the vicinity of the singular point, contrary to Tobak's hypothesis. Therefore, once again, the present results cannot confirm that a criterion exists for predicting the eventuality of singular separation.

4.2. Criteria for 3D ordinary flow separation

Determination of the three-dimensional ordinary flow separation location was successfully accomplished via visualization of free-flowing red blood cells. As expected, the projected area of the horseshoe vortex increased with increasing Reynolds number. Similarly, as verified through both

experimentation and numerical simulations, the magnitude of the wall shear stress inside the horseshoe region also increased as the Reynolds number increased. In agreement with oil streak experiments (Tobak & Peake, 1982), data gathered in this study point to the occurrence of three-dimensional flow separation when streamlines converge onto a particular surface separation line. Further, this surface separation line appears to originate from a singular point of zero wall shear stress. Thus, the origination of ordinary flow separation lines from a point of singular flow separation has been experimentally verified by the attached blood cell technique.

It has been shown mathematically and verified experimentally that the point of singular flow separation can be determined by identifying the point at which the two principal components of wall shear stress, τ_{yx} and τ_{yz} in this case, simultaneously vanish. For the flow around the vertical cylinder, both inside and outside of the vortex region, the magnitude of the wall shear stress increased as the fluid passed around the front of the cylinder, reached a maximum at the apex ($\theta = 90°$), and then decreased around the downstream side of the cylinder. Although the computational fluid dynamics simulation data are consistent with expected wall shear stress behavior, the data did not bring to light any connection between the magnitudes of the wall shear stress components and the location of the surface separation line. The qualitative and quantitative behavior of the wall shear stress inside and outside of the horseshoe vortex region was found to be consistent and continuous as the separation line was approached from either side.

The lack of any obvious connection between shear stress, pressure, and regular separation led to the examination of well-known yield criteria from the solid mechanics literature. The yield criteria chosen, the Tresca and the von Mises (Courtney, 1990; Dowling, 1999), provide a measure of the maximum and average difference in stress components, respectively. Calculation of the Tresca and von Mises stresses using the data from the three-dimensional flow geometry resulted in no observable connection between the characterized stresses and the location, or even the existence, of the surface separation line. In this sense, a recognizable analogy between solid mechanics and fluid mechanics does not appear to exist for flow separation.

5. Conclusion

A novel experimental technique incorporating surface-attached canine red blood cells as mechanical tracers to measure wall shear stress in regions of flow separation has been developed. The stress-elongation curve for red blood cells in this work is qualitatively similar to that obtained in other studies. This study, however, is the first to implement image analysis software to quantify the cell deformation. The use of such software added accuracy and increased sensitivity to the task of quantifying wall shear stress in laminar flow. This enabled the accurate measurement of wall shear stress as well as the determination of reversed flow regions in complex geometric flow conditions.

The wall shear stress was successfully quantified via cell deformation in the regions of flow separation and attachment. The technique used to determine wall shear stress proved to maintain high accuracy and sensitivity as the line of separation/attachment was approached. Accurate wall shear stress measurements were made as close as 0.15 mm to the apparent point or line of separation/attachment. The low range sensitivity limit for the attached red blood cells was approximately 0.5 dyn/cm^2; shear stress values below this lower limit were not accurately predicted via this technique.

The convergence of streamlines onto a single line has been confirmed as a criterion for three-dimensional flow separation. Whether this condition is sufficient for three-dimensional separated flow in general is not known, but it has been shown that the separation lines originate from singular separation points and it is the singular points that are both necessary and sufficient for separation to occur. No mathematical connection was apparent between the existence and location of the surface separation line (ordinary separation line), and either the magnitude of the total shear stress or the individual components of the stress. However, an effective experimental technique to aid in the further exploration of such an issue has been established and continued investigation may elicit such a relationship, or further support the absence of one.

Along the line of symmetry in a three-dimensional flow, the numerical results revealed the occurrence of a local pressure minimum preceding the point of flow separation. It was numerically confirmed that the

point of separation was not coincident with any extrema in the components of the pressure gradient. Numerical calculations revealed that singular flow separation in three dimensions was accompanied by a vanishing normal component of the surface pressure gradient, which corresponded to a vanishing streamwise derivative of the surface vorticity.

References

Ackerman, J. D., Wong, L., Ethier, C. R., Allen, D. G., & Spelt, J. K. (1994). Preston-static tubes for the measurement of wall shear stress. *Journal of Fluids Engineering*, *116*, 645.

Baker, C. J. (1979). The laminar horseshoe vortex. *Journal of Fluid Mechanics*, *95*, 347.

Baker, C. J. (1991). The oscillation of horseshoe vortex systems. *Journal of Fluids Engineering*, *113*, 489.

Cherukat, P., McLaughlin, J., & Dandy, D. S. (1999). A computational study of the inertial lift on a sphere in a linear shear flow field. *International Journal of Multiphase Flow*, *25,* 15.

Coon, M. D., & Tobak, M. (1995). Experimental study of saddle point of attachment in laminar juncture flow. *AIAA Journal*, *33*, 2288.

Courtney, T. H. (1990). *Mechanical Behavior of Materials*. New York: McGraw Hill.

Dandy, D. S., & Dwyer, H. A. (1990). A sphere in shear flow at finite Reynolds number: effect of particle lift, drag, and heat transfer. *Journal of Fluid Mechanics*, *219*, 381.

Dowling, N. E. (1999). *Mechanical Behavior of Materials: Engineering Methods for Deformation, Fracture, and Fatigue* (2nd ed.). New Jersey: Prentice Hall.

Gür, Y., & Leehey, P. (1989). A new wall shear stress gauge. *Experiments in Fluids*, *8*, 145.

Haguwara, Y., Esmaeilzadeh, E., Tsutsui, H., & Suzuki, K. (1989). Simultaneous measurement of liquid film thickness, wall shear stress and gas flow turbulence of horizontal wavy two-phase flow. *International Journal of Multiphase Flow*, *15*, 421.

Hardy, R. C., & Cottington, R. L. (1949). Measurements on the viscosity of water. *Journal of Research NBS, 42,* 573.

Hayashi, K., Yanai, Y., & Nakai, T. (1996). 3D-LDA study of the relation between wall shear stress and intimal thickness in human aortic bifurcation. *Journal of Biomechanical Engineering*, *118*, 273.

Henshaw, W. D. (1998). A primer for writing PDE solvers with Overture. Report no. LA-UR-96-3894. Los Alamos National Laboratory, Los Alamos, NM.

Hochmuth, R. M., Mohandas, N., & Blackshear, P. L., Jr. (1973). Measurement of the elastic modulus for red cell membrane using a fluid mechanical technique. *Biophysical Journal*, *13*, 747.

Hung, T. C., Shen, L. W., Akutsu, T., & Hwang, N. H. C. (1978). Some physical characteristics of normal erythrocyte membrane from experimental animals and humans. *Transactions American Society for Artificial Internal Organs, 24*, 573.

Kaul, U. K., Kwak, D., & Wagner, C. (1985). A computational study of saddle point separation and horseshoe vortex system. AIAA Paper 85-0182.

Kiehm, P., Mitra, N. K., & Fiebig, M. (1986). Numerical investigation of two- and three-dimensional confined wakes behind a circular cylinder in a channel. AIAA Paper 86-0035.

Kwak, D., Rogers, S. E., Kaul, K. K., & Chang, J. L. C. (1986). A numerical study of incompressible juncture flows. NASA-TM-88319.

Lee, D., & Chiu, J. J. (1992). A numerical simulation of intimal thickening under shear in arteries. *Biorheology*, *29*, 337.

Lee, D., Chiu, Y. L., & Jen, C. J. (1997). Platelet adhesion onto the wall of a flow chamber with an obstacle. *Biorheology*, *34*, 111.

Rakow, A. L., & Hochmuth, R. M. (1975a). Thermal transition in the human erythrocyte membrane: effect on elasticity. *Biorheology*, *15*, 1.

Rakow, A. L., & Hochmuth, R. M. (1975b). Effect of heat treatment on the elasticity of human erythrocyte membrane. *Biophysical Journal*, *15*, 1095.

Rogers, S. E., Kaul, U., & Kwak, D. (1986). A numerical study of single and multiple LOX posts and its application to the space shuttle main engine. AIAA Paper 86-0353.

Tobak, M., & Peake, D. J. (1982). Topology of three-dimensional separated flows. *Annual Reviews of Fluid Mechanics*, *14*, 61.

Tobak, M. (1997). Topologically derived separation onset conditions for two- and three-dimensional laminar flows. 35th Aerospace Science Meeting, AIAA 97-0866.

Wangard, W. (1999). Personal communication.

White, F. M. (1986). *Fluid Mechanics* (2nd ed.). New York: McGraw-Hill.

Williams, J. C. (1977). Incompressible boundary-layer separation. *Annual Reviews of Fluid Mechanics*, *9*, 113.

Yamaguchi, T., & Hanai, S. (1987). Measured wall shear stress distribution pattern upstream and downstream of a unilateral stenosis by an electrochemical method. *Biorheology*, *24*, 753.

Figure Captions

1. Schematic illustrating two common types of attachment for elongated red blood cells exposed to increasing wall shear.
2. An exploded view of the flow chamber used in the two- and three-dimensional flow experiments.
3. Experimental data collected for cell elongation $\lambda = L / L_o$ as a function of wall shear stress, τ_w. Each symbol, with an error bar representing ± 1 standard deviation, is the average elongation of 15 to 20 attached red blood cells. The dashed line is a fourth-order polynomial fit to the experimental data.
4. Streamlines predicted by numerical simulation for two-dimensional flow past a horizontal, cylindrical obstacle, at $Re = 23.9$.
5. Wall separation and attachment locations as a function of Reynolds number for the two-dimensional geometry. The solid symbols denote experimental measurements while the open symbols are the result of a flow simulation; the dashed lines are included for clarity.
6. Wall shear stress versus position in channel at a Reynolds number of 23.9, for the two-dimensional geometry. The solid symbols denote experimental measurements while the open symbols are the result of a flow simulation.
7. A top view of the flow around a vertical cylinder at $Re = 31.5$. (a) photograph of the immobilized and suspended cells; (b) projection of the near-surface streamlines determined by the three-dimensional flow simulation.
8. A magnified view of the cell deformation at the front of the cylinder within the horseshoe vortex region. A point of singular flow separation is seen to exist on the line of symmetry at the upstream edge of the vortex region.
9. The dimensionless position of the upstream singular separation point as a function of Re for the three-dimensional flow geometry.

10. Wall shear stress versus position in channel at a Reynolds number of 31.5, for the three-dimensional geometry. The solid symbols denote experimental measurements while the open symbols are the result of a flow simulation.
11. The magnitude of the wall shear stress for $Re = 44.1$ at different locations along the ordinary separation line. The angle is measured with respect to the upstream line of symmetry.
12. The total pressure at the wall along the line of symmetry, in the vicinity of the singular separation point at $Re = 44.1$. The separation point does not coincide with the extremum in the x-component of the pressure gradient.
13. The normal pressure gradient, $P_y \equiv \partial P/\partial y$, along the line of symmetry in the vicinity of the singular separation point $x = -0.08$ cm, or $x/D = -0.99$, at a Reynolds number of 44.1.
14. The wall shear stress, τ_w, and normal component of the pressure gradient, P_y, near the point of upstream flow separation in the two-dimensional flow geometry. For this case, $Re = 44.6$, separation occurs at $x/D = -0.65$.
15. The wall shear stress, τ_w, and the normal component of the pressure gradient, P_y, near the point of upstream flow separation along the line of symmetry in the three-dimensional flow geometry. In this case, $Re = 44.1$, separation occurs at $x/D = -0.99$.

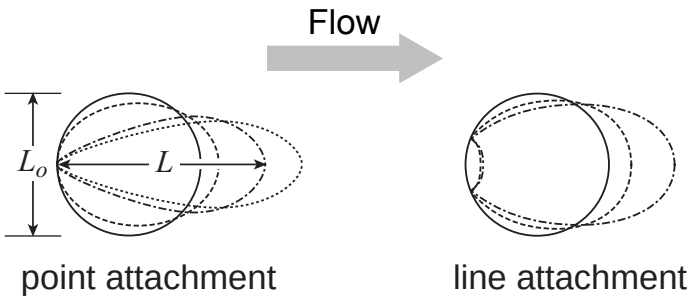

Figure 1

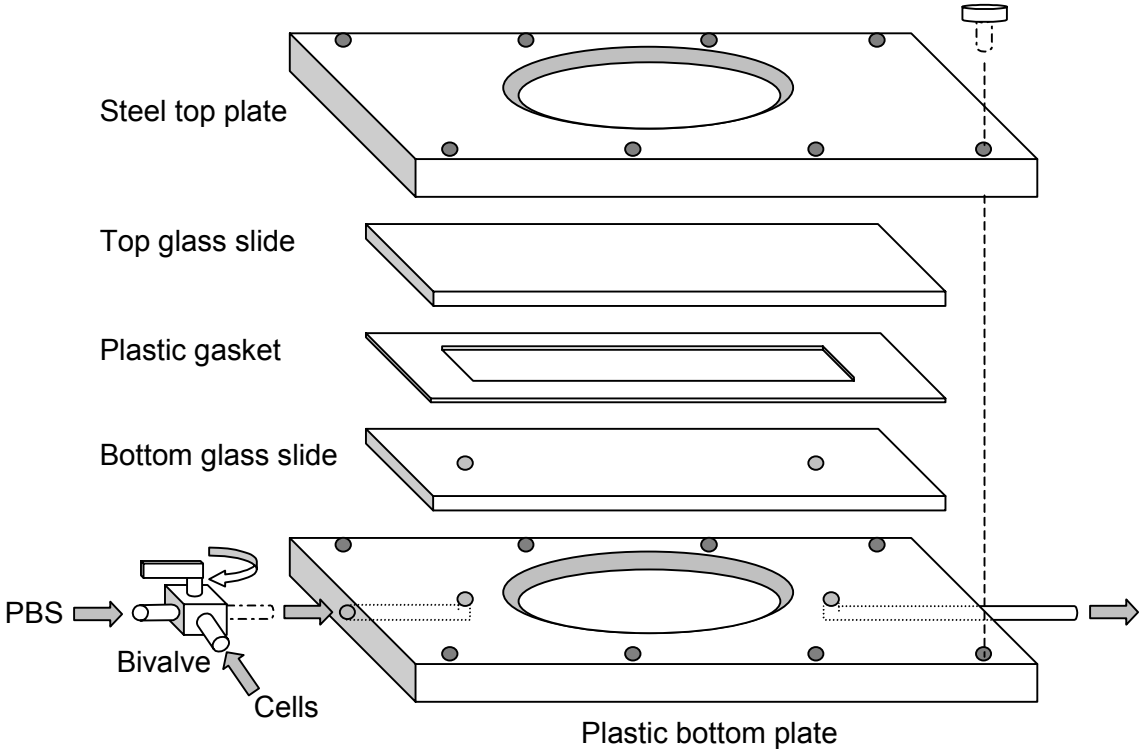

Figure 2

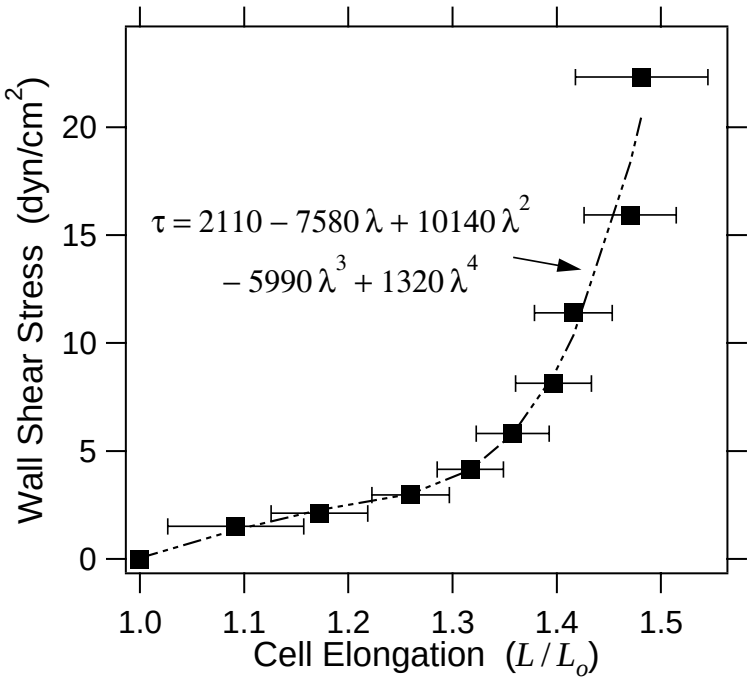

Figure 3

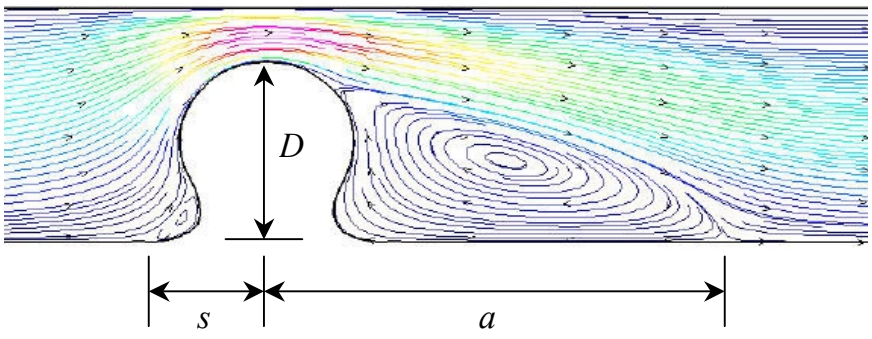

Figure 4

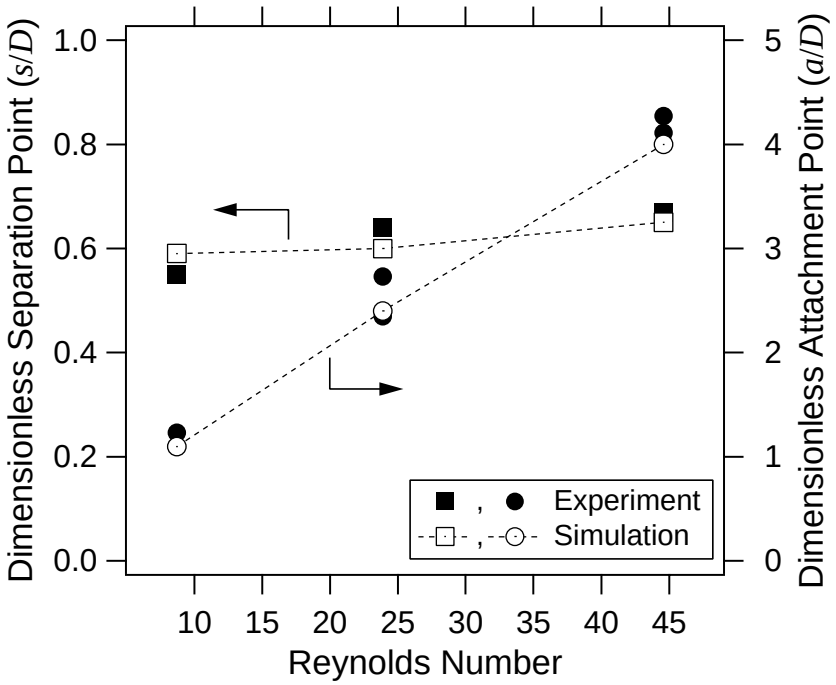

Figure 5

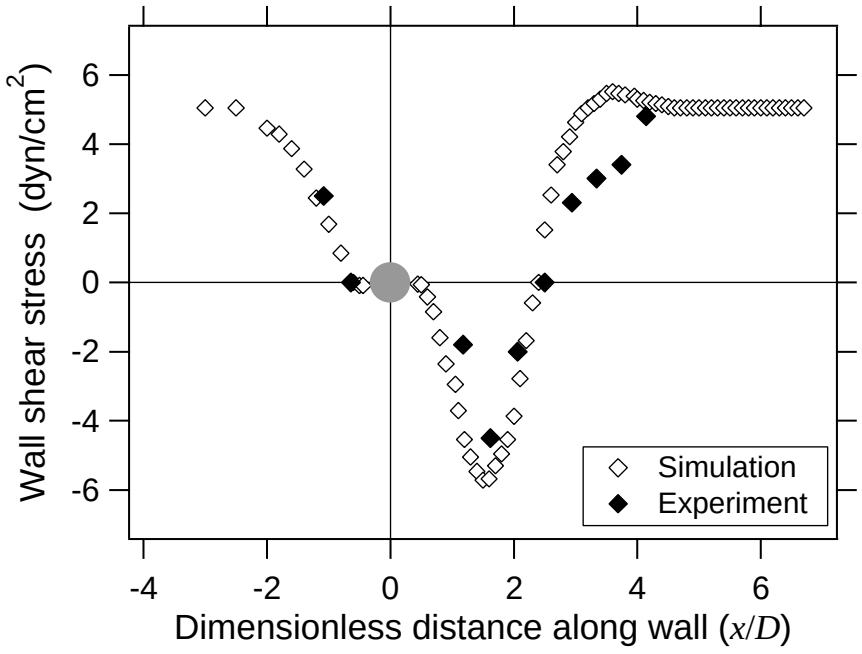

Figure 6

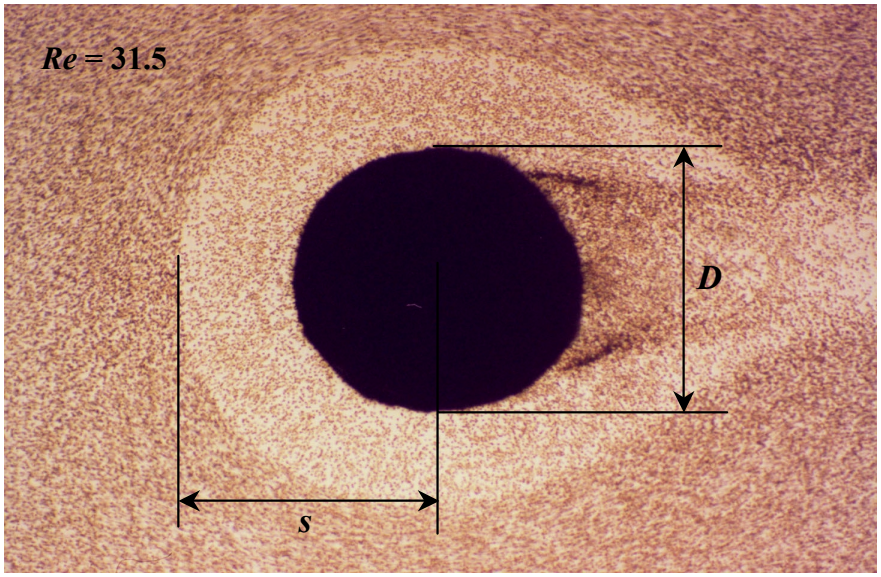

(a)

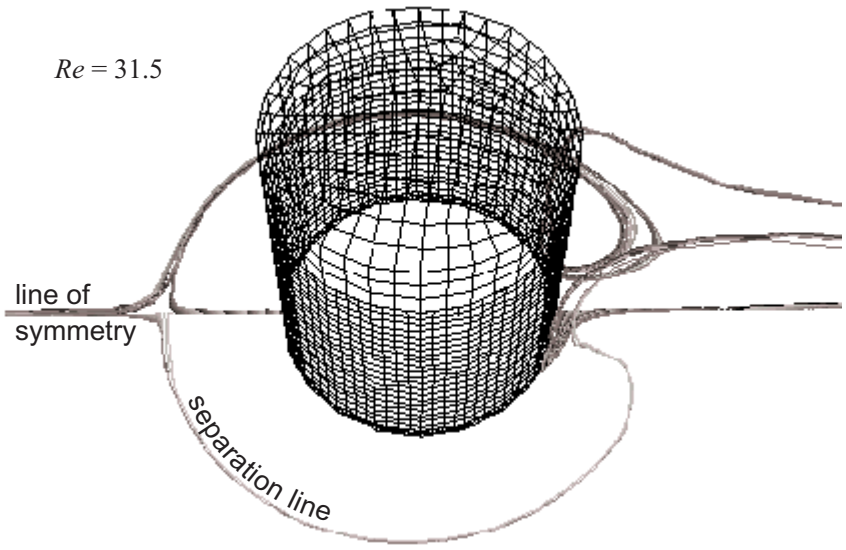

(b)

Figure 7

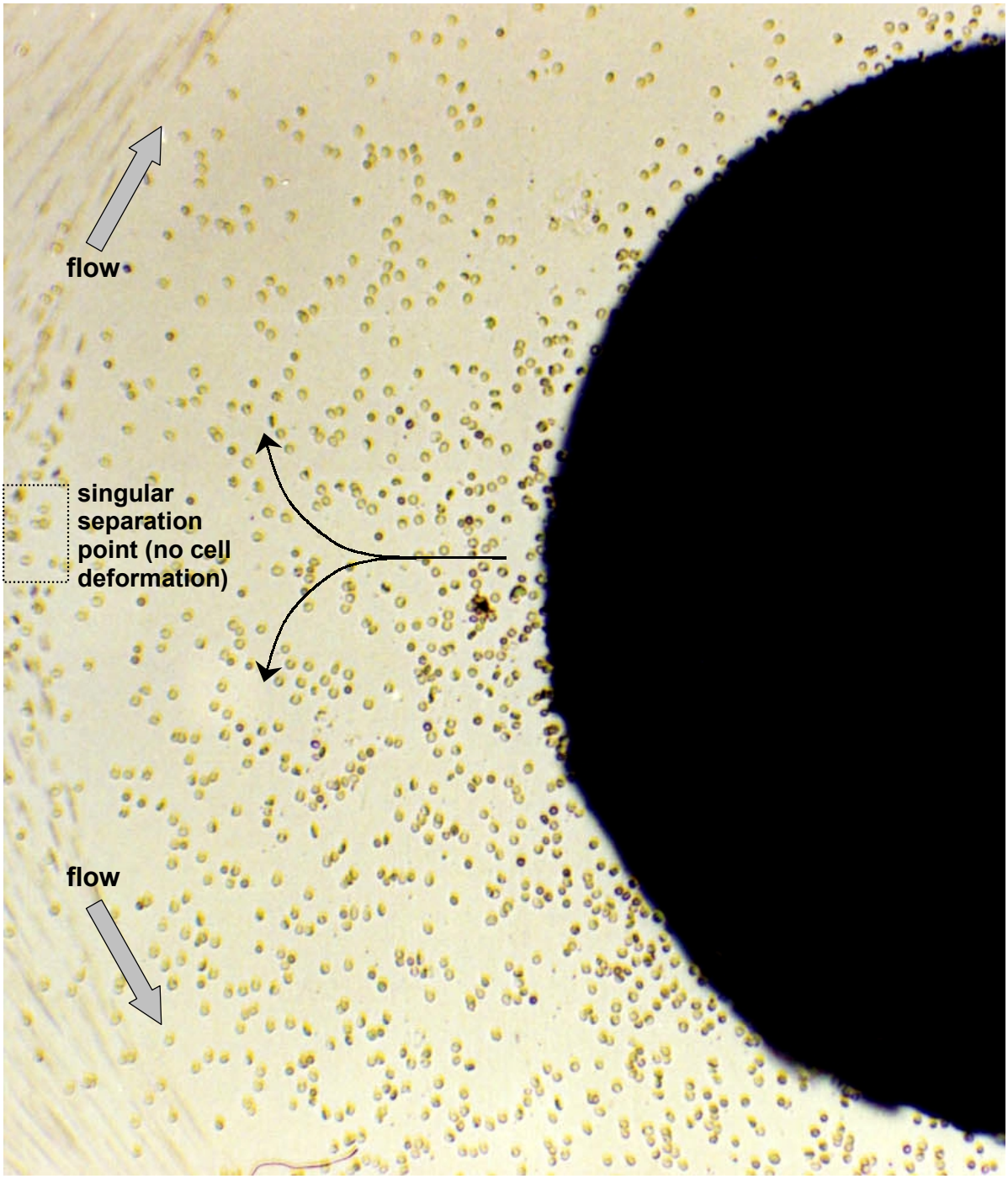

Figure 8

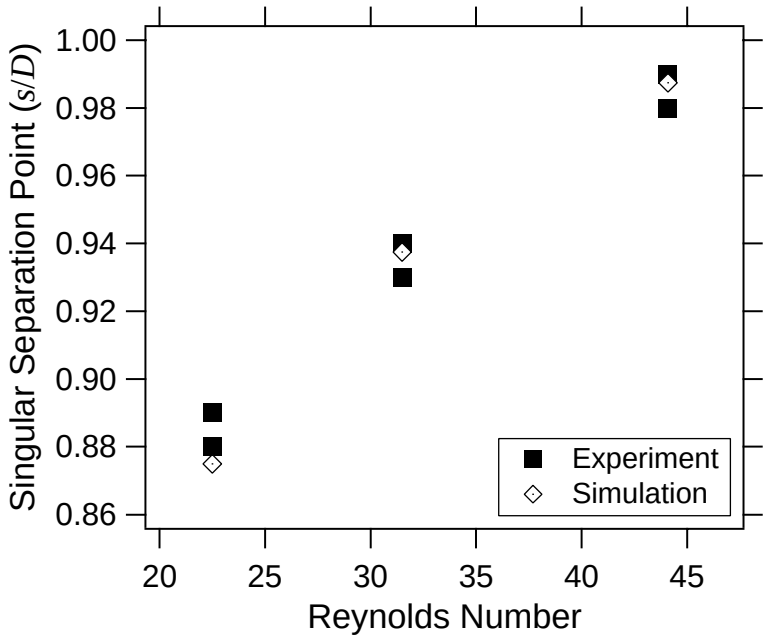

Figure 9

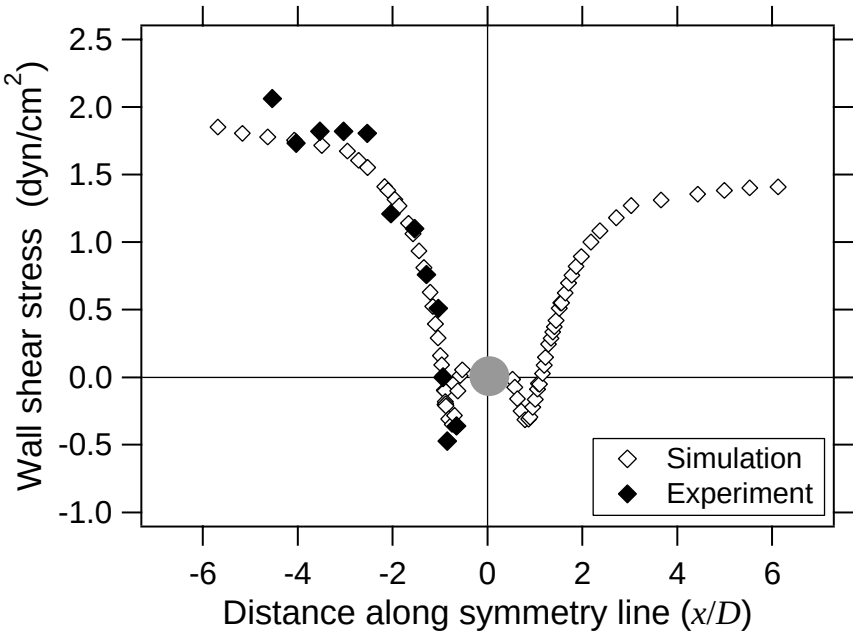

Figure 10

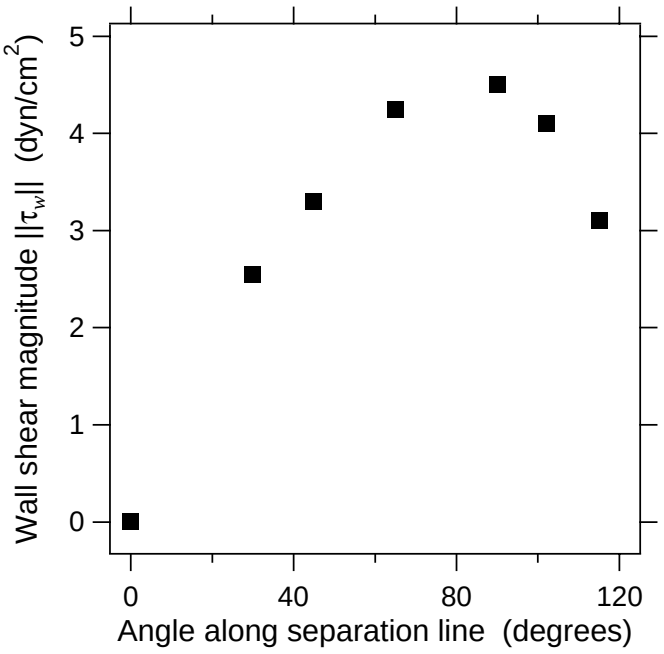

Figure 11

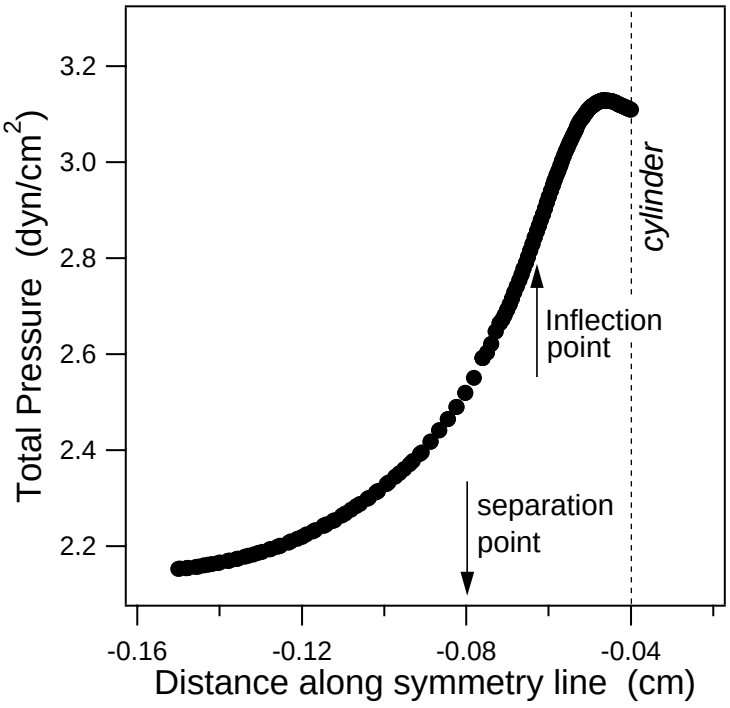

Figure 12

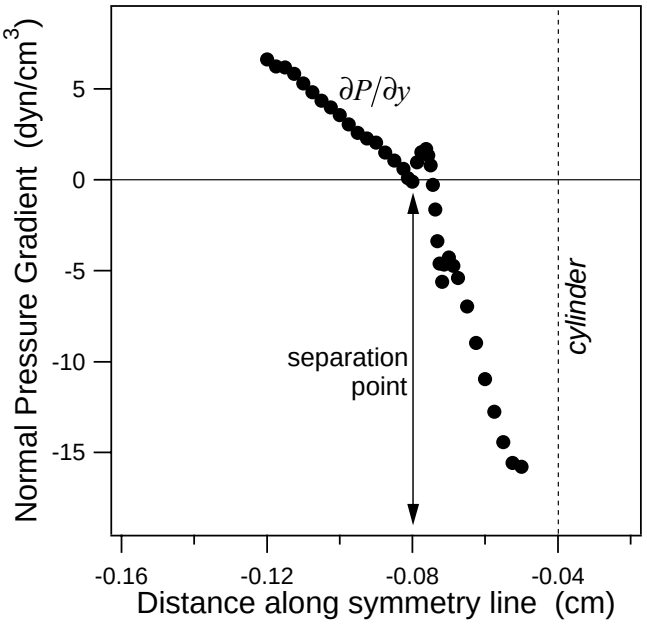

Figure 13

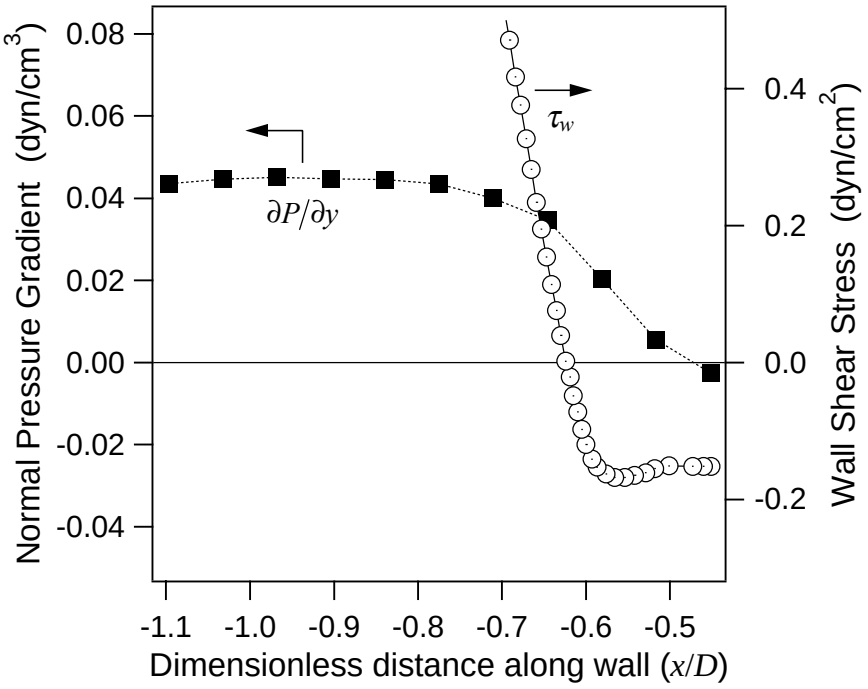

Figure 14

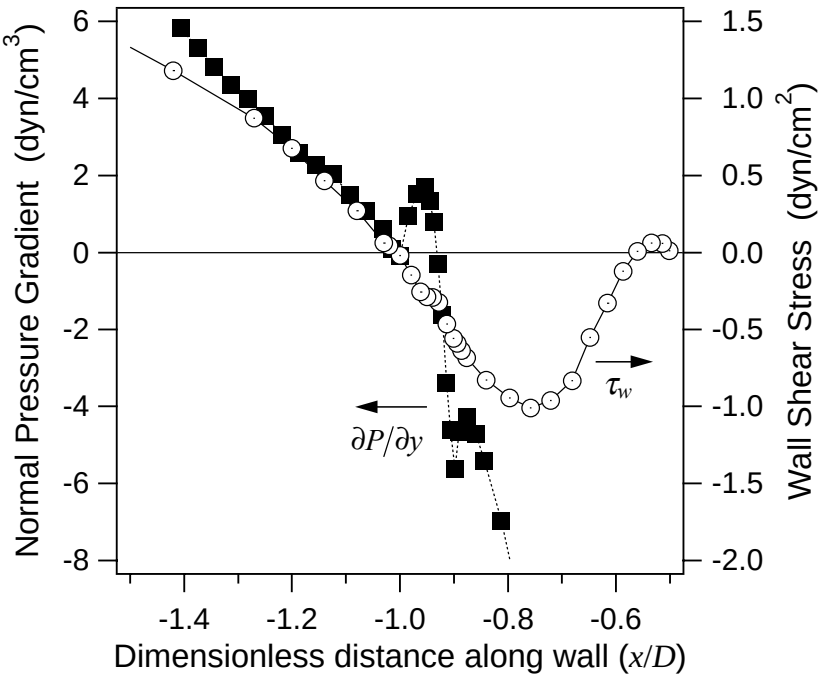
Normal Pressure Gradient (dyn/cm3)
Wall Shear Stress (dyn/cm2)
Dimensionless distance along wall (x/D)
∂P/∂y
τw
6
4
2
0
-2
-4
-6
-8
1.5
1.0
0.5
0.0
-0.5
-1.0
-1.5
-2.0
-1.4
-1.2
-1.0
-0.8
-0.6

Figure 15